expected to be the same for the entire perturbation series and, therefore, it does not affect the estimate of the LFER slope. Fast blockade by acetylthiocholine (more pronounced than that of choline) was relieved by depolarizing the patch to ~+50 mV. For the agonist series of Fig. 3, clusters of single-channel activity were defined over a range of ligand concentrations, k_+ was estimated from the saturating-concentration limit of the opening rate, and α was estimated from kinetic modelling, as described[25]. Concentrations up to 2 mM were used for ACh and carbamylcholine, up to 5 mM for tetramethylammonium and (4-keto-pentyl) trimethylammonium, up to 10 mM for formylcholine (FCh) and acetylthiocholine and up to 20 mM for all other agonists. In the case of unliganded •S268T AChRs (Fig. 4), where openings did not occur in clusters, continuous stretches of data were idealized (program SKM) and gating rate constants were estimated using the program MIL (f_c = 18 kHz; dead time = 20 • s). The programs are available from www.qub.buffalo.edu.

To avoid the uncertainty associated with the calculation of activation-barrier heights from rate constants, we used log k versus log K plots instead of $\Delta G^{\ddagger}$ versus ΔG° plots. • values were calculated from the slope of linear fits to such plots ('Brønsted' plots).

Received 6 September; accepted 26 November 1999.

1. Leffler, J. E. & Grunwald, E. *Rates and Equilibria of Organic Reactions* (Wiley, New York, 1963).
2. Kyte, J. *Mechanism in Protein Chemistry* 461–519 (Garland, New York, 1995).
3. Fersht, A. R., Leatherbarrow, R. J. & Wells, T. N. C. Quantitative analysis of structure–activity relationships in engineered proteins by linear free-energy relationships. *Nature* **322**, 284–286 (1986).
4. Leffler, J. E. Parameters for the description of transition states. *Science* **117**, 340–341 (1953).
5. Jaffé, H. H. A reexamination of the Hammett equation. *Chem. Rev.* **53**, 191–261 (1953).
6. Kirsch, J. F. in *Advances in Linear Free Energy Relationships* (eds Chapman, N. B. & Shorter, J.) 369–400 (Plenum, London, 1972).
7. Estell, D. A. *et al.* Probing steric and hydrophobic effects on enzyme–substrate interactions by protein engineering. *Science* **233**, 659–663 (1986).
8. Fersht, A. R., Leatherbarrow, R. J. & Wells, T. N. Structure–activity relationships in engineered proteins: analysis of use of binding energy by linear free energy relationships. *Biochemistry* **26**, 6030–6038 (1987).
9. Toney, M. D. & Kirsch, J. F. Direct Brønsted analysis of the restoration of activity to a mutant enzyme by exogenous amines. *Science* **243**, 1485–1488 (1989).
10. Eaton, W. A., Henry, E. R. & Hofrichter, J. Application of linear free energy relations to protein conformational changes: the quaternary structural change of hemoglobin. *Proc. Natl Acad. Sci. USA* **88**, 4472–4475 (1991).
11. Yifrach, O. & Horovitz, A. Mapping the transition state of the allosteric pathway of GroEL by protein engineering. *J. Am. Chem. Soc.* **120**, 13262–13263 (1998).
12. Fersht, A. R. Characterizing transition states in protein folding: an essential step in the puzzle. *Curr. Opin. Struct. Biol.* **5**, 79–84 (1995).
13. Onuchic, J. N., Socci, N. D., Luthey-Schulten, Z. & Wolynes, P. G. Protein folding funnels: the nature of the transition state ensemble. *Folding Design* **1**, 441–450 (1996).
14. Edelstein, S. J., Schaad, O., Henry, E., Bertrand, D. & Changeux, J. P. A kinetic mechanism for nicotinic acetylcholine receptors based on multiple allosteric transitions. *Biol. Cybern.* **75**, 361–379 (1996).
15. Ortells, M. O. & Lunt, G. G. Evolutionary history of the ligand-gated ion-channel superfamily of receptors. *Trends Neurosci.* **18**, 121–127 (1995).
16. Karlin, A. & Akabas, M. H. Toward a structural basis for the function of nicotinic acetylcholine receptors and their cousins. *Neuron* **15**, 1231–1244 (1995).
17. Magleby, K. L. & Stevens, C. F. The effect of voltage on the time course of end-plate currents. *J. Physiol.* **223**, 151–171 (1972).
18. Auerbach, A., Sigurdson, W., Chen, J. & Akk, G. Voltage dependence of mouse acetylcholine receptor gating: different charge movements in di-, mono- and unliganded receptors. *J. Physiol.* **494**, 155–170 (1996).
19. Monod, J., Wyman, J. & Changeux, J. P. On the nature of allosteric transitions: a plausible model. *J. Mol. Biol.* **12**, 88–118 (1965).
20. Itzhaki, L. S., Otzen, D. E. & Fersht, A. R. The structure of the transition state for folding of chymotrypsin inhibitor 2 analyses by protein engineering methods: evidence for nucleation–condensation mechanism for protein folding. *J. Mol. Biol.* **254**, 260–288 (1995).
21. Sunderman, E. R. & Zagotta, W. N. Sequence of events underlying the allosteric transition of rod cyclic nucleotide-gated channels. *J. Gen. Physiol.* **113**, 621–640 (1999).
22. Jackson, M. B. Spontaneous openings of the acetylcholine receptor channel. *Proc. Natl Acad. Sci. USA* **81**, 3901–3904 (1984).
23. Straub, J. E. & Karplus, M. The interpretation of site-directed mutagenesis experiments by linear free energy relations. *Protein Eng.* **3**, 673–675 (1990).
24. Hammett, L. P. in *Advances in Linear Free Energy Relationships* (eds Chapman, N. B. & Shorter, J.) vii (Plenum, New York, 1972).
25. Hamill, O. P., Marty, A., Neher, E., Sakmann, B. & Sigworth, F. J. Improved patch-clamp techniques for high-resolution current recording from cells and cell-free membrane patches. *Pflügers Arch.* **391**, 85–100 (1981).
26. Salamone, F. N., Zhou, M. & Auerbach, A. A re-examination of adult mouse nicotinic acetylcholine receptor channel activation kinetics. *J. Physiol.* **516**, 315–330 (1999).
27. Qin, F., Auerbach, A. & Sachs, F. Estimating single-channel kinetic parameters from idealized patch-clamp data containing missed events. *Biophys. J.* **70**, 264–280 (1996).
28. Akk, G., Zhou, M. & Auerbach, A. A mutational analysis of the acetylcholine receptor channel transmitter binding site. *Biophys. J.* **76**, 207–218 (1999).
29. Akk, G., Sine, S. & Auerbach, A. Binding sites contribute unequally to the gating of mouse nicotinic alpha D200N acetylcholine receptors. *J. Physiol.* **496**, 185–196 (1996).
30. Zhou, M., Engel, A. G. & Auerbach, A. Serum choline activates mutant acetylcholine receptors that cause slow channel congenital myasthenic syndromes. *Proc. Natl Acad. Sci. USA* **96**, 10466–10471 (1999).
31. Wang, H.-L. *et al.* Acetylcholine receptor M3 domain: stereochemical and volume contributions to channel gating. *Nature Neurosci.* **2**, 226–233 (1999).

Acknowledgements

This work was supported by grants from the NIH (A.A.) and the Myasthenia Gravis Foundation of America Inc. (C.G. and A.A.). We thank J. Richard, F. Sachs and S. Sine for discussions and critical comments, and F. Salamone and K. Lau for technical assistance.

Correspondence and requests for materials should be addressed to C.G. (e-mail: grosman@buffalo.edu). or A.A. (e-mail: auerbach@buffalo.edu).

Positional cloning of zebrafish *ferroportin1* identifies a conserved vertebrate iron exporter

Adriana Donovan*, Alison Brownlie*†, Yi Zhou*, Jennifer Shepard*, Stephen J. Pratt‡, John Moynihan*, Barry H. Paw*, Anna Drejer*, Bruce Barut*†, Agustin Zapata§, Terence C. Law‖, Carlo Brugnara‖, Samuel E. Lux*, Geraldine S. Pinkus¶, Jack L. Pinkus¶, Paul D. Kingsley#, James Palis#, Mark D. Fleming*¶, Nancy C. Andrews*† & Leonard I. Zon*†

* *Department of Medicine, Division of Hematology / Oncology, Children's Hospital and Dana-Farber Cancer Institute, Boston, Massachusetts 02115, USA*
† *Howard Hughes Medical Institute, Children's Hospital, Boston, Massachusetts 02115, USA*
‡ *Washington University School of Medicine, St. Louis, MO 63110, USA*
§ *Department of Cell Biology, Faculty of Biology, Complutense University, 28040 Madrid, Spain*
‖ *Department of Laboratory Medicine, Children's Hospital, Boston, Massachusetts 02115, USA*
¶ *Department of Pathology, Brigham and Women's Hospital, Boston, Massachusetts 02115, USA*
# *Department of Pediatrics and Cancer Center, University of Rochester Medical Center, Rochester, New York 14642, USA*

Defects in iron absorption and utilization lead to iron deficiency and overload disorders. Adult mammals absorb iron through the duodenum, whereas embryos obtain iron through placental transport. Iron uptake from the intestinal lumen through the apical surface of polarized duodenal enterocytes is mediated by the divalent metal transporter, DMT1 (refs 1–3). A second transporter has been postulated to export iron across the basolateral surface to the circulation. Here we have used positional cloning to identify the gene responsible for the hypochromic anaemia of the zebrafish mutant *weissherbst*. The gene, *ferroportin1*, encodes a multiple-transmembrane domain protein, expressed in the yolk sac, that is a candidate for the elusive iron exporter. Zebrafish *ferroportin1* is required for the transport of iron from maternally derived yolk stores to the circulation and functions as an iron exporter when expressed in *Xenopus* oocytes. Human Ferroportin1 is found at the basal surface of placental syncytiotrophoblasts, suggesting that it also transports iron from mother to embryo. Mammalian Ferroportin1 is expressed at the basolateral surface of duodenal enterocytes and could export cellular iron into the circulation. We propose that Ferroportin1 function may be perturbed in mammalian disorders of iron deficiency or overload.

Two independent autosomal recessive mutations of the zebrafish hypochromic blood mutant *weissherbst* (*weh*), *weh*^{th238} and *weh*^{tp85c} were isolated as part of a large-scale screen for ethyl nitrosourea (ENU)-induced mutations that disrupt embryonic development in zebrafish[4]. These *weh* mutants were identified in a morphologic screen for defects in circulating erythroid cells[5]. The number of circulating erythroid cells of both mutant alleles are normal at 33

and 48 hours post fertilization (h.p.f.), but the *weh* mutant cells are hypochromic (lacking red colour) (data not shown). Mutant embryos have little, if any, haemoglobin compared with wild-type embryos at 33 h.p.f. and 48 h.p.f. (Fig. 1a, *o*-dianisidine stain), but some haemoglobin is detectable at 72 h.p.f. The weh^{th238} allele has less *o*-dianisidine staining compared with the weh^{tp85c} allele at 72 h.p.f. (data not shown), indicating that it may be a more severe allele. In addition to the hypochromia, a progressive decrease in red cell number occurs after 48 h.p.f. By 96 h.p.f., the number of circulating erythroid cells in mutants decreases to ~20% of the number in the wild type (data not shown). The *weh* mutant cells at days 2 and 3 have a large nucleus and basophilic cytoplasm characteristic of more immature erythroid cells, and on day 5 the remaining mutant cells are misshapen (Fig. 1b). Further studies of erythroid differentiation reveal that embryonic globin messenger RNA levels are abnormally maintained during maturation (Fig. 1a). Although *weh* mutants have no gross organ defects in addition to their anaemia, all mutant embryos die between day 7 and day 14 of development (data not shown).

Given the possibility that hypochromia could result from iron deficiency, we measured iron levels in *weh* erythroid cells. The level of iron measured in 10^4 wild-type cells ranged from 0.093 ng to 0.208 ng ($n = 3$), whereas the levels of iron in the same number of *weh* mutant cells ranged from 0.014 ng to 0.033 ng ($n = 3$). The 4–9-fold decrease in erythrocyte iron levels could be due to low levels of iron in circulation. As confirmation of this hypothesis, iron-dextran injected intravenously into weh^{tp85c} mutant embryos completely rescued haemoglobin production (Fig. 1c). This rescue shows that *weh* mutant erythroid cells are fully capable of haemoglobinization, and that the hypochromia is caused by inadequate circulatory iron levels.

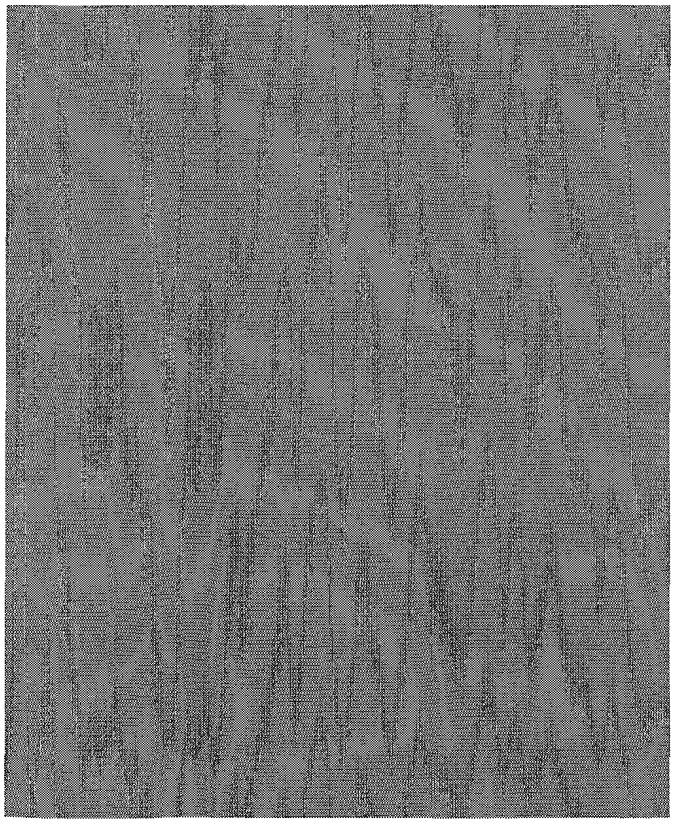

Figure 1 Phenotypic analysis of *weissherbst* (*weh*) mutants. **a**, Detection of haemoglobin (*o*-dianisidine staining) and • e2-globin mRNA (whole embryo *in situ* hybridization) in wild-type and mutant embryos at 33 hours post fertilization (h.p.f.), 48 h.p.f. and 72 h.p.f. **b**, Wright–Giemsa staining of circulating embryonic erythroid cells from wild-type and weh^{tp85c} embryos on day 2 (56 h.p.f.), day 3 (80 h.p.f.) and day 5 (125 h.p.f.). **c**, Injection of iron–dextran into weh^{tp85c} mutants. Embryos were stained for haemoglobin (*o*-dianisidine) at 80 h.p.f.

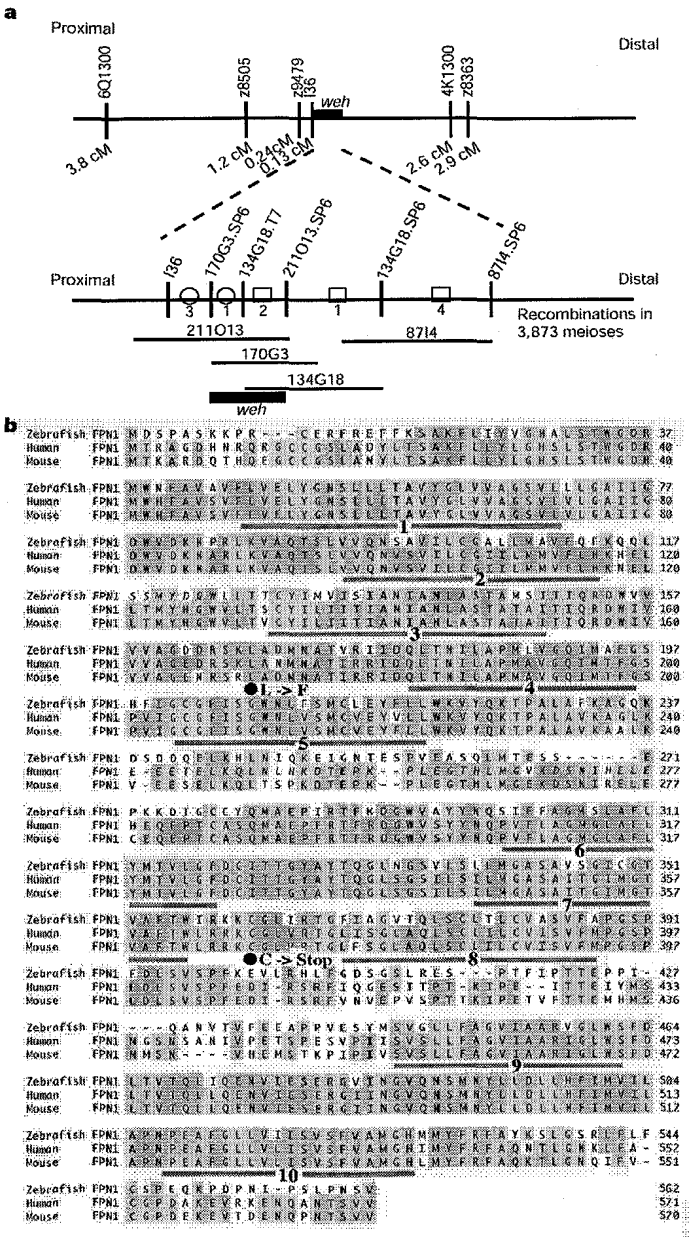

Figure 2 Positional cloning of the *weissherbst* gene. **a**, The *weh* locus is depicted by a thick black bar just distal to the AFLP marker I36. Below is an enlarged view of the *weh* locus that depicts the BAC and PAC genomic clones identified by a chomosomal walk in an analysis of 3,873 meioses. Genotyping of a total of 1,783 meioses from haploid animals and 2,090 meioses from diploid mutants narrowed the critical interval containing the gene to the PAC clones 211O13 and 170G3. The numbers of recombination events identified on the proximal side (circles) and distal side (squares) of the *weh* locus are indicated. **b**, Sequence alignment of zebrafish, human and mouse Ferroportin1 (FPN1). The initiator methionine in all three species was established by the presence of upstream, in-frame stop codons. Identical amino acids (yellow), predicted transmembrane domains (red bars below sequence), and mutations identified in the weh^{tp85c} and weh^{th238} alleles (black circles below sequence) are indicated.

To gain further insight into this phenotype, we isolated the *weh* mutant gene by positional cloning methods. Study of the segregation of centromeric microsatellite markers in half-tetrad gynogenetic diploid embryos localized *weh* to linkage group 9 (data not shown). Genetic mapping placed the *weh* locus in an ~6 cM interval between the random amplified polymorphic DNA (RAPD) markers 4K1300 and 6Q1300 (Fig. 2a). We isolated more closely linked markers using amplified fragment length polymorphism (AFLP) analysis (data not shown)[6,7], scanning ~10,000 polymorphic loci. Single-strand conformational polymorphism analysis showed that the AFLP marker I36 was 0.13 cM proximal to the *weh* locus (Fig. 2a).

A chromosomal walk towards the gene was initiated from the I36 marker (Fig. 2a), which resulted in the identification of a critical interval that contained the *weh* gene (Fig. 2a). In an attempt to identify potential candidates for the *weh* gene, we used a hybridization strategy to screen complementary DNA libraries for genes located on the PAC clones identified in the region of the *weh* locus. We hybridized a radiolabelled insert of PAC clone 170G3 to zebrafish gridded cDNA libraries. Screening of 100,000 gridded cDNA clones identified five clones of a new cDNA, designated *WC1* (for *weh* cDNA 1). Analysis of *WC1* mRNA expression in embryos and sequencing *WC1* from weh^{th238} mutants suggested that *WC1* was not a candidate for *weh* (data not shown). Two genes, *STAT1* and *glutaminase*, were isolated by hybridization of the zebrafish PAC clone 87I4 (Fig. 2a) to gridded cDNA libraries (data not shown). The human orthologues of *WC1*, *STAT1* and *glutaminase* are localized to human chromosome 2 in a 2.4 cM interval (data not shown), showing conserved chromosomal synteny among vertebrates[8]. Homology searches identified a pufferfish (*Fugu rubripes*) cosmid clone (121D21) that contained both *WC1* and *STAT1* (data not shown). This cosmid also contained *Fugu* homologues of other genes located on human chromosome 2. Using primers designed to the pufferfish sequence of one of these genes (121D21aB3), a 200-base pair (bp) fragment of the zebrafish orthologue was amplified from PAC 211013. A full-length cDNA (3.7 kb) of this gene, hereafter referred to as *ferroportin1*, was isolated from a zebrafish kidney cDNA library.

This gene, *ferroportin1*, has a predicted open reading frame of 562 amino acids (Fig. 2b). Sequence analysis of the weh^{th238} allele identified a C-to-A nucleotide transversion that causes premature termination of translation at codon 361 (Fig. 2b). Similar analysis of the weh^{tp85c} allele identified a single amino-acid change, Leu167→Phe, resulting from a G-to-T nucleotide difference (Fig. 2b). The finding of a premature stop mutation in weh^{th238} strongly suggests that the *weh* mutant phenotype is caused by a defect in *ferroportin1*. Mouse and human *ferroportin1* cDNA clones were obtained by polymerase chain reaction with reverse transcriptase (RT-PCR) of RNA isolated from liver and placenta, respectively. A conserved sequence, predicted to form a hairpin-loop structure typical of iron response elements[9], was identified in the 5′ untranslated region (UTR) of the cDNAs from all three species (data not shown). On the basis of protein structure-prediction analysis, Ferroportin1 contains at least 10 transmembrane segments (Fig. 2b).

In situ hybridization analysis of zebrafish embryos shows that *ferroportin1* mRNA is not expressed in erythroid cells. *Ferroportin1* mRNA is detected at 18 h.p.f. through 48 h.p.f. in the yolk syncytial layer (YSL) (Fig. 3a). The YSL is the peripheral layer of the yolk cell that lies just below the membrane[10]. This layer surrounds the entire yolk of the embryo and consists of yolk-free cytoplasm and nuclei. Yolk has been shown to contain nutrients needed during development[11], including iron[11–13] (L.I.Z., unpublished data). Embryos express *ferroportin1* in the region of the YSL at 18 h.p.f. (Fig. 3a, arrow) that lies just below the developing haematopoietic cells in the intermediate cell mass[14]. At 48 h.p.f., *ferroportin1* is expressed in a localized region of the YSL (Fig. 3a, arrowhead). Expression is in the same region of the YSL over which the blood flows[15]. At both time-points, *ferroportin1* is expressed in the region of the YSL adjacent to the blood, but not by the entire YSL. This pattern of expression suggests that *ferroportin1* expression and function in the YSL are linked to red blood cell development. Considering the iron–dextran rescue of haemoglobin production in *weh* mutants, the YSL expression of *ferroportin1* suggested that the gene might function in the transport of iron from the yolk to the embryonic circulation.

To determine that defects in the *ferroportin1* gene cause the *weh* mutant phenotype, we injected a plasmid that expresses Ferroportin1 fused to green fluorescent protein (GFP) into the yolk cell between the 256-cell and 1,000-cell stages[10]. After 48 hours of development, 33% of injected embryos expressed GFP strictly in the YSL. At 80 h.p.f., the phenotype of mutant embryos expressing GFP was compared to the uninjected mutants. The Ferroportin1–GFP-expressing mutant embryos ($n = 9$) had considerably more haemoglobin expression than uninjected mutants (Fig. 3b). This partial rescue of the hypochromia provides further evidence that *ferroportin1* is the *weh* gene, and shows that Ferroportin1 acts in the

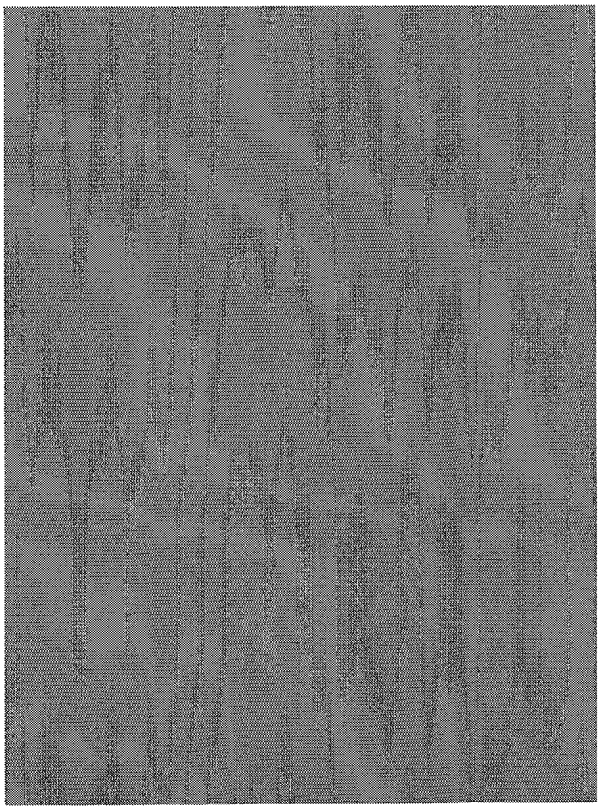

Figure 3 Developmental expression of *Ferroportin1* and phenotypic rescue of *weh* embryos. **a**, Whole embryo mRNA *in situ* hybridization analysis for *ferroportin1* at 18 and 48 h.p.f. Dark purple stain indicates expression of *ferroportin1*. Expression is seen in the YSL of embryos at both 18 and 48 h.p.f., and in the brain at 48 h.p.f. **b**, Phenotypic rescue of *weh* mutant embyros. Offspring of weh^{th238} heterozygote animals injected in the YSL with a plasmid expressing Ferroportin1–GFP. Embryos were stained with *o*-dianisidine at 80 h.p.f. to detect haemoglobin. **c**, Iron efflux measured in *Xenopus* oocytes. Oocytes expressing either DMT1 alone or DMT1 and FPN1 were loaded with ^{55}Fe by incubation in uptake buffer containing 60 • m $^{55}FeCl_2$. Efflux from individual oocytes was measured by incubation of oocytes in 500 • l of efflux buffer with or without 20 mg ml^{-1} apo-transferrin (– apoTfr and + apoTfr). After efflux, the total ^{55}Fe content of both the efflux solution and the individual oocytes was measured by scintillation counting. The data are expressed as an average ($n = 6$) of the ratio of the picomoles of efflux to the picomoles of uptake per oocyte.

YSL. The rescue of the *weh* mutant phenotype by intravenous iron–dextran injection and by Ferroportin1 expressed in the YSL indicates that Ferroportin1 functions to deliver yolk iron into the embryonic circulation.

We tested the function of Ferroportin1 using a *Xenopus* oocyte expression system. Because the proposed function of Ferroportin1 is to export iron, we needed to first load the oocytes with ^{55}Fe. Radioactive iron loading was accomplished through the expression of the iron transporter DMT1 in oocytes and then loading of ^{55}Fe at pH 5.5. ^{55}Fe-loaded oocytes that expressed either DMT1 alone or DMT1 and Ferroportin1 were tested for iron export activity either in the presence or absence of apo-transferrin, an iron chelator. To normalize for the iron content in each individual oocyte, the ratio of efflux to uptake was calculated. Our results showed that, in the presence of apo-transferrin, the efflux to uptake ratio in oocytes expressing Ferroportin1 was fivefold greater than control oocytes not expressing Ferroportin1 (Fig. 3c, P • 0.001).

To evaluate a potential role for *ferroportin1* in iron transport in mammals, we examined tissue expression. Northern blot analysis showed that the highest levels of expression are in human placenta, liver, spleen and kidney (Fig. 4a). In mice, *ferroportin1* mRNA is expressed specifically in the duodenum but not in the jejunum or ileum (Fig. 4b). Additionally, *ferroportin1* is expressed in the large intestine. Most intestinal iron absorption occurs in the proximal duodenum, placing *ferroportin1* in a physiologically appropriate location to function in intestinal iron absorption. Messenger RNA *in situ* hybridization analysis was carried out on sections of mouse embryos. The primitive erythroblasts derived from the blood islands do not express *ferroportin1*, whereas the trophoblast cells of the inner placenta (Fig. 4c) express high levels of *ferroportin1* RNA. Within the embryo proper, *ferroportin1* transcripts are detected in several tissues, particularly in the gut and liver (Fig. 4d). The expression of *ferroportin1* in placenta, duodenum and liver, all prominent sites of iron transport, is consistent with the proposed role of the gene in iron transport.

To characterize the expression of Ferroportin1 protein, we generated a specific polyclonal antibody. In the human placenta, Ferroportin1 protein was primarily expressed in a basal location within the syncytiotrophoblasts (Fig. 4e). The basal surface of the syncytiotrophoblast interfaces with the fetal circulation, whereas the apical surface contacts the maternal circulation. The mammalian placenta and the zebrafish YSL provide a homologous function, serving as the site of iron transfer between mother and embryo. These results, together with the functional data in zebrafish and *Xenopus*, indicate that Ferroportin1 probably exports iron from the syncytiotrophoblast into the embryonic circulation.

A similar analysis of mouse duodenum showed Ferroportin1 staining in enterocytes in the villus (Fig. 4g). The intensity of staining was stronger at the tip of the villus compared with the crypt. Staining was particularly strong at the basolateral surface of

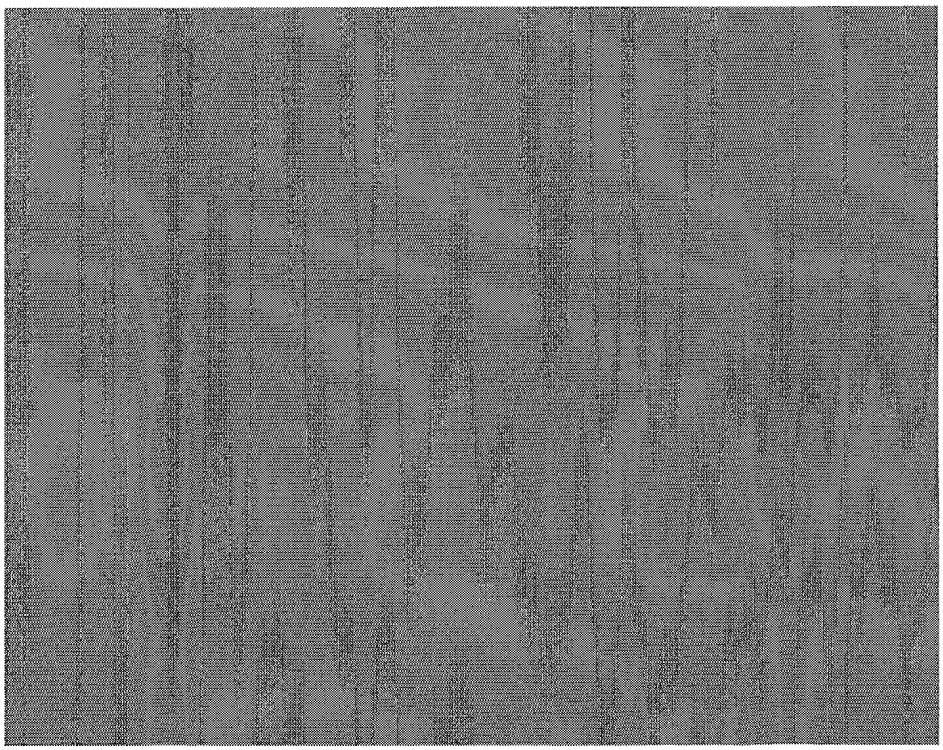

Figure 4 *Ferroportin1* expression in human and mouse tissues. **a**,**b**, Northern blots of adult human tissues (**a**) and mouse intestinal segments (**b**) probed with human or mouse *ferroportin1*, respectively (top panel) and mouse • -actin (lower panel). Sk, skeletal; Per. bl. leuk., peripheral blood leukocytes. **c**, mRNA *in situ* hybridization study of E12.5 mouse embryo and placenta. *Ferroportin1* transcripts are in the inner placenta (labyrinth zone, lz) and the trophoblast giant cells (arrow) at the border between the outer placenta (spongiotrophoblast, s), but not in the maternal deciduum (d). *Ferroportin1* expression is also present in the visceral endoderm of the yolk sac (ys) surrounding the embryo proper. **d**, Sagittal section of E14.5 mouse embryo. Within the embryo, *ferroportin1* expression is evident in the liver (li) and the internal and herniated gut (hg), as well as in the vascular plexus (vp) surrounding the central nervous system. Scale bars, 1 mm (**c**,**d**). **e–i**, Immunohistochemical staining of human and mouse tissues with a Ferroportin1 peptide antibody. **e**, Human placenta stained by immunoperoxidase staining (brown staining) using an affinity purified, anti-human Ferroportin1 polyclonal rabbit antiserum (original magnification ×100). The arrow indicates basal localization of staining in the syncytiotrophoblast. F, fetal circulation; M, maternal circulation. **f**, Human liver (original magnification ×100). Note strong staining of Kupffer cell (arrow). Hepatocytes (H) are also positive. **g**, Mouse duodenum (original magnification ×40). T, tip of villus; C, crypt. **h**,**i**, Higher magnification of duodenal enterocytes at the tip of the villus. Note complete lack of staining at the apical brush border (black arrow) and prominent basolateral staining (arrows with asterisk).

the enterocyte (Fig. 4h,i). The duodenal enterocytes of the small intestine are polarized epithelial cells that transport iron into the intestinal capillaries through the basolateral membrane. The mechanism of intestinal basolateral iron transport has not been established. Sex-linked anaemia (*sla*) mice have a defect in basolateral iron transport in the duodenum as deduced from ferrokinetic studies and the presence of abnormal iron deposits in duodenal enterocytes[16]. Analogous to *weh* mutants, the *sla* mouse has a defect in transport of maternal iron to the embryonic circulation[17]. The *sla* phenotype is due to a mutation in the membrane-bound multicopper ferroxidase gene, *hephaestin*[18]. In *Saccharomyces cerevisiae*, the hephaestin-like ferroxidase *FET3* is required for high-affinity iron uptake by the iron transporter *FTR1* (refs 19, 20). Expression of Ferroportin1 at the basolateral surface of duodenal enterocytes in mouse and the multiple-transmembrane structure of the protein make it an excellent candidate to function as a basolateral iron transporter.

Additional data from the *weh* mutant suggests that Ferroportin1 functions in the intestine of the adult zebrafish. Both *in situ* hybridization studies and immunohistochemistry showed expression of zebrafish *ferroportin1* in the intestine (data not shown). In addition, iron–dextran-rescued mutant embryos live past the normal time of lethality (day 7–14). We have successfully raised these rescued embryos to adulthood. These fish are smaller than their wild-type siblings and have a profound hypochromic anaemia (data not shown). As these fish eat a normal diet replete in iron, but nonetheless are severely anaemic, these data suggest that the gene is required for intestinal iron absorption in addition to yolk sac transport. On the basis of the basolateral expression pattern of Ferroportin1 in mammalian enterocytes and the implication that *ferroportin1* is required for intestinal iron transport in zebrafish, the protein is probably involved in iron export from enterocytes in mammals. Further experiments are required to determine whether Ferroportin1 cooperates with hephaestin in these cells.

Other tissues may use *ferroportin1* as an iron exporter. Very high levels of expression are evident in Kupffer cells (Fig. 4f), the resident macrophages of the liver and macrophages located within the splenic red pulp (data not shown). Ferroportin1 might have a role in iron export from macrophages, a critical function in recycling of iron from senescent erythrocytes.

Iron is required for many cellular processes, but it can also be toxic when present in excess; thus, iron homeostasis must be strictly maintained. We have used zebrafish genetics to identify the multiple-transmembrane domain protein Ferroportin1, a new iron export protein. In the mammalian yolk sac and placenta, Ferroportin1 may have an important conserved role in the transport of iron from the maternal to the embryonic circulation. In adults, Ferroportin1 probably functions in iron transport at the basolateral surface of duodenal enterocytes. In disorders such as iron deficiency or overload, tissues respond by altering normal iron metabolism. Ferroportin1 might be involved in the pathophysiology of iron deficiency anaemias or iron overload syndromes, such as haemochromatosis.

Methods

Zebrafish strains and studies

Linkage analysis was performed on haploid or diploid embryos obtained from AB/DAR, AB/SJD or AB/WIK hybrids[21]. Wright–Giemsa and *o*-dianisidine staining of embryos were done as described[6]. *In situ* hybridization analysis was done as described[22].

Genetic mapping and genotyping and library screens

Linkage to centromeric markers[23] was carried out by half-tetrad analysis[24]. For fine genetic mapping, haploids were genotyped on the proximal side of the locus with one of the RAPD markers, 4W1600, 6Q1300 or 4AC800, and on the distal side with 4K1300 or O61020 (Operon Technologies). Diploid mutant embryos were genotyped on the proximal side with the microsatellite markers z8505 or z9479 and on the distal side with z8363 (ref. 25). All library screens were done as described[29].

In situ hybridization and rescue experiment embryos (see below) were genotyped using allele-specific oligonucleotide (ASO) hybridization assays[26,27] specific to the weh^{tp85c} and weh^{th238} *ferroportin1* alleles. The weh^{th238} oligonucleotides were developed to distinguish the C-to-A mutation in the weh^{th238} allele from the wild-type allele (wild-type 5′-AAAGAAGTGCGGCCTCATC-3′ and mutant 5′-AAAGAAGTGAGGCCTCATC-3′). The weh^{tp85c} oligonucleotides were developed to distinguish the G-to-T mutation in the weh^{tp85c} allele from the wild-type allele (wild-type 5′-GAGCAAATTGGCAGGTAAG-3′ and mutant 5′-GAGCAAATTTGCAGGTAAG-3′).

Isolation of the mouse and human *ferroportin1* cDNAs

Expressed sequence tag (EST) clones were identified that contained the 5′ end (GenBank accession number D63209) and 3′ end (GenBank W23461) of human *ferroportin1* and the 3′ end of mouse *ferroportin1* (GenBank AA500296). The coding region of human and mouse *ferroportin1* cDNAs were cloned by RT-PCR with a forward primer made to the conserved iron response element sequence in the 5′ UTR (5′-CAACTTCAGCTACAGTGTTAG-3′) and a reverse primer just 3′ of the stop codon of each cDNA (mouse 5′-TTATACAACAGATGTATTCGGT-3′ and human 5′-AACTGTCTCAAACAACAGATG-3′).

Embryo injection experiments

We created a zebrafish Ferroportin1–GFP fusion protein construct by PCR. The forward PCR primer contained the start codon, 5′-CCGCTCGAGAACGCACAATGGACAGCCCTG-3′. The reverse primer contained the last codon, 5′-CCGCTCGAGTACAGAGTTTGGAAGTGAGGG-3′. The PCR product was subcloned into the GFP expression vector pEGFP-N1 (Clontech). Embryos from a cross of two weh^{th238} heterozygotes were injected[21] with the Ferroportin1–GFP plasmid (300 ng ml^{-1}). For the iron–dextran rescue experiment, 48-h mutant embryos from a weh^{tp85c} cross were injected intravenously with an iron–dextran solution (100 mg ml^{-1}, Sigma).

Xenopus oocyte injections and ^{55}Fe efflux experiments

Complementary RNA for injection was prepared using the mMessage Machine kit (Ambion), using a construct containing either the rat *DMT1* cDNA in pSPORT1 (gift from H. Gunshin[2]) or the zebrafish *ferroportin1* cDNA in the vector pXT7 (gift from S. Sokol). Defollicularized oocytes were incubated in ND96 (96 mM NaCl, 2 mM KCl, 1.8 mM $CaCl_2$, 1 mM $MgCl_2$, 5 mM HEPES and 2.5 mM sodium pyruvate, pH 7.4) and injected with either 20 ng of *DMT1* cRNA alone or 20 ng each of both the *DMT1* and *ferroportin1* cRNAs. ^{55}Fe uptake and efflux were carried out 48 h after injection. ^{55}Fe uptake was performed in 500 • l of a solution containing 60 • M $^{55}FeCl_2$, 100 mM NaCl, 10 mM Hepes and 1 mM ascorbic acid at pH 5.5 for 30 minutes. ^{55}Fe uptake was stopped by incubation of the oocytes in 1 mM cold $FeCl_2$, 100 mM NaCl, 10 mM HEPES and 1 mM ascorbic acid, pH 6.0, for 30 min. Individual oocytes were placed in 500 • l of either efflux buffer (100 mM NaCl, 10 mM HEPES, pH 7.4) alone or efflux buffer containing a final concentration of 20 mg ml^{-1} apo-transferrin for 60 min. After incubation the ^{55}Fe levels of both the efflux solution and the individual oocytes lysed in 10% SDS were measured by scintillation counting.

Mouse *in situ* hybridization and northern blot analysis

In situ hybridization of murine embryos was performed as described[28]. An adult multiple-tissue human northern blot (Clontech) containing 2 • g of poly(A)$^+$ mRNA per lane was probed with a human *ferroportin1* EST (GenBank W05488). The mouse intestinal northern blot containing 20 • g of total RNA per lane was probed with a mouse *ferroportin1* EST (GenBank AA500296).

Antibodies and immunohistochemistry

A rabbit polyclonal antibody was generated to a peptide consisting of the C-terminal 19 amino acids of the human Ferroportin1 protein (Genemed Synthesis). Antiserum was affinity purified against the peptide. Formalin or Bouin's fixed paraffin-embedded specimens were deparaffinized and heat treated for 30 min in 1.0 mM EDTA, pH 8.0, in an HS80 steamer (Black and Decker). Endogenous peroxidase activity was quenched in methanol and 3% hydrogen peroxide (5:1, v/v). The slides were then incubated in 3% normal swine serum in 0.05 M Tris, pH 7.6, followed by rabbit anti-Ferroportin1 antibody (7 • g ml^{-1}), and sequentially in HRP-conjugated goat anti-rabbit immunoglobulins (1:40 dilution, Dako), HRP-conjugated rabbit anti-goat immunoglobulins (1:40 dilution, Dako), followed by HRP-conjugated swine anti-rabbit immunoglobulins (1:52 dilution, Dako), each prepared in 0.10 M Tris, pH 7.6, containing (4%) human AB serum. Antibody localization was determined using DAB in 0.5 M Tris (pH 7.6) containing (0.035%) hydrogen peroxide. Slides were counterstained with methyl green. Control samples were incubated with normal rabbit serum or purified rabbit immunoglobulins at a protein concentration equal to the antibody preparation. In addition, pre-incubation of the antibody with specific peptide at a 550-fold molar excess neutralized the reactivity.

Red cell iron measurement

Iron levels in red blood cells were measured by atomic absorption spectrometer model 3030 equipped with Zeeman graphite furnace and autosampler (Perkin Elmer). A cell sample (at least 30,000 cells in 20 • l PBS) or blank (PBS) was diluted with 40 • l of 480 mg dl^{-1} magnesium nitrate (matrix modifier); 20 • l of the mixture was injected into the instrument and analysed in duplicate. The instrument was calibrated with iron standards of 10, 25, 100 and 250 ng ml^{-1} prepared from Atomic Spectroscopy Standard (Perkin Elmer).

Structure prediction

Hydropathy plots (Kyte–Doolittle) were obtained using the Genetics Computer Group (GCG) programs PEPTIDESTRUCTURE and PEPPLOT with a hydropathy window of 14. Transmembrane amino-acid segments were identified and their topographies predicted using the programs PHDhtm (www.embl-heidelberg.de/predictprotein/predictprotein.html), HMMTOP (www.enzim.hu/hmmtop/), TMHMM (www.cbs.dtu.dk/services/TMHMM-1.0/), TMpred (www.ch.embnet.org/software/TMPRED_form.html), TopPred2 (www.biokemi.su.se/~server/toppred2/) and SOSUI (www.tuat.ac.jp/~mitaku/). Most analyses predict 10 transmembrane segments. Some predict that the first and last transmembrane segments are split and that Ferroportin contains 12 segments. Others predict that transmembrane segments 4 and 5 are not split and that only 9 segments are present.

Received 16 December 1999; accepted 19 January 2000.

1. Fleming, M. D. *et al.* Microcytic anemia mice have a mutation in Nramp2, a candidate iron transporter gene. *Nature Genet.* **16,** 383–386 (1997).
2. Gunshin, H. *et al.* Cloning and characterization of a mammalian proton-coupled metal-ion transporter. *Nature* **388,** 482–488 (1997).
3. Andrews, N. C. Disorders of iron metabolism. *N. Engl. J. Med.* **341,** 1986–1995 (1999).
4. Haffter, P. *et al.* The identification of genes with unique and essential functions in the development of the zebrafish, *Danio rerio*. *Development* **123,** 1–36 (1996).
5. Ransom, D. G. *et al.* Characterization of zebrafish mutants with defects in embryonic hematopoiesis. *Development* **123,** 311–319 (1996).
6. Ransom, D. G. & Zon, L. I. in *The Zebrafish: Genetics and Genomics* (eds Detrich, H. W. I., Westerfield, M. & Zon, L. I.) 195–210 (Academic, San Diego, 1999).
7. Vos, P. *et al.* AFLP: a new technique for DNA fingerprinting. *Nucleic Acids Res.* **23,** 4407–4414 (1995).
8. Postlethwait, J. H. *et al.* Vertebrate genome evolution and the zebrafish gene map. *Nature Genet.* **18,** 345–349 (1998).
9. Eisenstein, R. S. & Blemings, K. P. Iron regulatory proteins, iron responsive elements and iron homeostasis. *J. Nutr.* **128,** 2295–2298 (1998).
10. Kimmel, C. B., Ballard, W. W., Kimmel, S. R., Ullmann, B. & Schilling, T. F. Stages of embryonic development of the zebrafish. *Dev. Dyn.* **203,** 253–310 (1995).
11. Richards, M. P. Trace mineral metabolism in the avian embryo. *Poult. Sci.* **76,** 152–164 (1997).
12. Dumont, J. N. Oogenesis in *Xenopus laevis* (Daudin). VI. The route of injected tracer transport in the follicle and developing oocyte. *J. Exp. Zool.* **204,** 193–217 (1978).
13. Craik, J. C. Levels of calcium and iron in the ovaries and eggs of cod *Gadus morhua L.* and plaice *Pleuronectes platessa* L. *Comp. Biochem. Physiol. A.* **83,** 515–517 (1986).
14. Al-Adhami, M. A. & Kunz, Y. W. Ontogenesis of haematopoietic sites in *brachydanio rerio* (Hamilton–Buchanan) (Teleostei). *Develop. Growth Differ.* **19,** 171–179 (1977).
15. Rieb, J.-P. La circulation sanguine chez l'embryon de *Brachydanio rerio*. *Annales d'Embryologie et de Morphogenese* **6,** 43–54 (1973).
16. Bannerman, R. M. Genetic defects of iron transport. *Fed. Proc.* **35,** 2281–2285 (1976).
17. Kingston, P. J., Bannerman, C. E. & Bannerman, R. M. Iron deficiency anaemia in newborn *sla* mice: a genetic defect of placental iron transport. *Br. J. Haematol.* **40,** 265–276 (1978).
18. Vulpe, C. D. *et al.* Hephaestin, a ceruloplasmin homologue implicated in intestinal iron transport, is defective in the *sla* mouse. *Nature Genet.* **21,** 195–199 (1999).
19. Askwith, C. *et al.* The *FET3* gene of *S. cerevisiae* encodes a multicopper oxidase required for ferrous iron uptake. *Cell* **76,** 403–410 (1994).
20. Stearman, R., Yuan, D. S., Yamaguchi-Iwai, Y., Klausner, R. D. & Dancis, A. A permease–oxidase complex involved in high-affinity iron uptake in yeast. *Science* **271,** 1552–1557 (1996).
21. Westerfield, M. *The Zebrafish Book* (Univ. Oregon Press, Eugene, 1993).
22. Thompson, M. A. *et al.* The *cloche* and *spadetail* genes differentially affect hematopoiesis and vasculogenesis. *Dev. Biol.* **197,** 248–269 (1998).
23. Knapik, E. W. *et al.* A microsatellite genetic linkage map for zebrafish. *Nature Genet.* **18,** 338–343 (1998).
24. Johnson, S. L., Africa, D., Horne, S. & Postlethwait, J. H. Half-tetrad analysis in zebrafish: mapping the *ros* mutation and the centromere of linkage group I. *Genetics* **139,** 1727–1735 (1995).
25. Shimoda, N. *et al.* Zebrafish genetic map with 2000 microsatellite markers. *Genomics* **58,** 219–232 (1999).
26. Farr, C. J., Saiki, R. K., Erlich, H. A., McCormick, F. & Marshall, C. J. Analysis of RAS gene mutations in acute myeloid leukemia by polymerase chain reaction and oligonucleotide probes. *Proc. Natl Acad. Sci. USA* **85,** 1629–1633 (1988).
27. Wood, W. I., Gitschier, J., Lasky, L. A. & Lawn, R. M. Base composition-independent hybridization in tetramethylammonium chloride: a method for oligonucleotide screening of highly complex gene libraries. *Proc. Natl Acad. Sci. USA* **82,** 1585–1588 (1985).
28. Palis, J. & Kingsley, P. D. Differential gene expression during early murine yolk sac development. *Mol. Reprod. Dev.* **42,** 19–27 (1995).
29. Brownlie, A. *et al.* Positional cloning of the zebrafish *sauternes* gene: a model for congenital sideroblastic anaemia. *Nature Genet.* **20,** 244–250 (1998).

Acknowledgements

We thank J. Amatruda, C. Trenor, V. Sellers and J. Levy for critical review of this manuscript; P. Haffter and C. Nusslein-Volhard for providing the zebrafish blood mutants before publication; C. Amemiya, J. Postlethwait, D. Nathan, A. Oates and J. Best for helpful discussions and experimental advice; D. Giarla for administrative assistance; B. Hogan, J. Rossant and L. Solnica-Krezel for discussions on placental and yolk sac biology; and L. Kunkel, G. Gilliland and W. Talbot for support and advice. L.I.Z. and N.C.A. are Associate Investigators of the Howard Hughes Medical Institute. This work was supported by grants from the NIH.

Correspondence and requests for materials should be addressed to L.I.Z. (e-mail: zon@rascal.med.harvard.edu).

cDNA sequences have been deposited in GenBank under accession codes AA226612 (zebrafish *ferroportin1*), AA226614 (human *ferroportin1*) and AA226613 (mouse *ferroportin1*).

Interaction between Wnt and TGF-β signalling pathways during formation of Spemann's organizer

Michiru Nishita*†, Minako K. Hashimoto†‡, Souichi Ogata‡, Micheline N. Laurent‡§, Naoto Ueno*, Hiroshi Shibuya* & Ken W. Y. Cho‡

* *Division of Morphogenesis, Department of Developmental Biology, National Institute for Basic Biology, Okazaki 444-8585, Japan*
‡ *Department of Developmental and Cell Biology, University of California, Irvine, California 92617-2300, USA*
† *These authors contributed equally to this work*
§ *Present address: Department of Biology, California Institute of Technology, 1200E. California Boulevard, Pasadena, California 91125, USA*

Members of the Wnt and TGF-β superfamilies regulate both cell fate and proliferation during development and tissue maintenance[1–3]. In the early amphibian embryo, the Wnt and TGF-β superfamily signalling cascades are required for the establishment of a dorsal signalling centre, Spemann's organizer[4–8]. Intracellular proteins of both pathways, upon activation, translocate to the nucleus to participate in transcription. Here we show that β-catenin and Lef1/Tcf, which are downstream components of the Wnt signalling cascade, form a complex with Smad4, an essential mediator of signals initiated by members of the TGF-β growth factor superfamily. In *Xenopus*, this interaction directly and synergistically affects expression of the *twin* (*Xtwn*) gene during formation of the organizer. This is, to our knowledge, the first

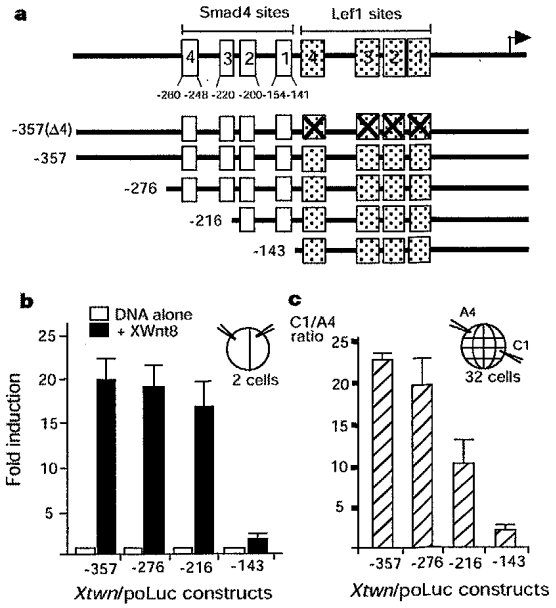

Figure 1 Deletion analysis of *Xtwn* reporter genes. **a**, Deletion constructs used for animal cap and blastomere injection assays. Putative Smad4 (open boxes: 5′-GTCT-3′ (ref. 13)) and Lef1 (shaded boxes) binding sites are indicated. Sites 1, 2 and 3 are consensus Lef1/Tcf binding sites previously identified[9], and site 4 is a newly identified non-consensus Lef1 site (AAGATCAAGGG; see Fig. 2d). Mutation of all four Lef1 binding sites generated −357(Δ4)*Xtwn*/Luc. Smad boxes 1, 2, 3 and 4 fall within the indicated three GST–Smad4MH1-protected regions. **b**, Deletion from −216 to −143 markedly reduces the Wnt responsiveness of the *Xtwn* promoter. **c**, Blastomere injection assay. A single A4 or C1 blastomere was injected at the 32-cell stage with the indicated deletion constructs. Fold induction relative to background (A4 levels of activity) is indicated.